Formation and Morphology of M_7C_3 in Low Cr White Iron Alloyed With Mn and Cu

Vinod Kumar

(Submitted 7 November 2002; in revised form 20 November 2002)

The presence of M_7C_3 carbide in white iron enhances its wear resistance because of high hardness. Scanning electron microscopy (SEM) revealed its morphology as a pencil-like hexagonal structure. On the basis of the SEM observations, elemental distribution studies, and differential thermal analysis (DTA) of some heat-treated hypoeutectic white irons alloyed with Cr, Mn, and Cu, it is concluded that M_7C_3 carbides form as a result of attainment of a favorable condition in the liquid phase present at the austenite grain boundaries. Segregation of phosphorus in the intercellular regions and formation of a copper-rich intermetallic is responsible for the formation of this liquid phase. Austenite was found to nucleate first, followed by the nucleation and growth of M_7C_3 carbide in its vicinity, because of rejection of C and Cr during formation of austenite. The rosette structure generally observed is formed from the joining of M_7C_3 carbides by precipitation of secondary carbides.

Keywords Cr white iron, M_7C_3 carbide, morphology, wear/abrasion

1. Introduction

M_7C_3 provides good resistance to wear/abrasion because of high hardness[1] and therefore, forms the basis for the development of wear/abrasion-resistant alloys. M_7C_3 may form directly from the liquid as primary carbides or may precipitate as secondary carbides from austenite because of a decrease in solubility of carbon in austenite with a decrease in temperature. The secondary M_7C_3 may nucleate on the existing M_7C_3 or as separate nuclei. Laird et al.[2] carried out the fractal analysis of carbide morphology in high-Cr white irons and observed that a hyper-eutectic alloy first solidifies via $L \rightarrow M_7C_3$, forming nucleation sites for the subsequent growth of M_7C_3 during eutectic reaction. As such, this alloy consists mainly of the faceted hexagonal-shaped carbides. A near-eutectic alloy first solidifies as $L \rightarrow \gamma Fe$ (austenite) with the subsequent eutectic reaction occurring within large pools of liquid. As such, faceted hexagonal-shaped carbides are allowed unrestricted growth among the rosette-type clusters formed by the eutectic reaction $L \rightarrow M_7C_3 + \gamma Fe$. This consists of mixed morphology of smooth facets from the hexagonal-shaped carbides and coarse facets of the quasi-rectangular and blade-like carbides. A hypoeutectic alloy experiences prior growth of γFe (austenite) which interdendritically constrains the growth of the M_7C_3 phase during the eutectic reaction $L \rightarrow M_7C_3 + \gamma Fe$.

The precipitate morphology is controlled by (1) minimization of interfacial free energy in a given volume fraction of precipitate, and (2) the total elastic energy (taking into account both the components involving precipitate-matrix and precipitate-precipitate interactions) associated with nucleation and growth.[3] Local constraints to growth may further affect the shape of the precipitates.[3-6]

Hunt and Jackson[7] classified the eutectic solidification as lamellar nonfaceted-nonfaceted, faceted-nonfaceted, or faceted-faceted on the basis of a phase being classified according to a dimensionless factor α. A lamellar eutectic will form where both phases have an α value of <2. If a phase has a high α value (>2), its growth as a eutectic constitute will produce a faceted interface. Metal-metal carbide eutectics fall into the faceted-nonfaceted phase and the carbide is the faceted phase.[8] According to this classification, the austenite-M_7C_3 eutectic would not be expected to be lamellar.[9]

Pearce[10] observed that the hexagonal-shaped M_7C_3 resembles a pencil-like structure and showed that the central core was martensite. Pearce[10] suggested that the growth of eutectic M_7C_3 may occur in a manner similar to that proposed by Ohide et al.[11] for primary crystals, which are believed to form as a hexagonal shell and grow inward with a remaining melt or shrinkage cavity at the central zone of the hexagonal form. This suggests that the nucleation of M_7C_3 took place away from the core and grew inward, thereby leaving a molten core with low concentration of C and Cr. The core liquid later transformed to austenite and then into martensite because the Ms temperature increased as a result of low C and Cr.[12] According to this observation, formation of M_7C_3 took place similarly to the casting process in which solidification starts at the mold surface and precedes inward and the core solidifies in the end. For this process, nucleation sites similar to a mold wall must be present in the liquid, which is only a hypothetical case and is never possible in reality.

In view of the above discussion, an effort has been made to study the formation sequence and morphology of hexagonal-shaped M_7C_3. An explanation is presented about the formation of a pencil-like structure of M_7C_3.

2. Experimental Procedures

The alloy was air-melted in clay-bonded graphite crucibles in an induction furnace and sand cast into 25-mm diameter ×

Vinod Kumar, Product Development Division, R & D Centre for Iron & Steel, Steel Authority of India Limited, Ranchi (Jharkhand), 834 002 India. Contact e-mail: sp@rdcis.bih.nic.in.

Table 1 Alloy Composition, wt.%

C	S	P	Si	Mn	Cr	Cu
3.05	0.070	0.183	2.24	6.1	4.8	1.46

250-mm-long cylindrical ingots. Chemical analysis (Table 1) was done with the help of a vacuum quantimeter and x-ray fluorescence analysis.

Heat treatments comprised soaking at 800, 850, 900, 950, 1000, and 1050 °C for 2, 4, 6, 8, and 10 h followed by air-cooling. Heat treatments were carried out in an airtight muffle furnace, the temperature of which was controlled within ±5 °C.

Optical metallography was done on disc samples (height ≈ 15 mm) that were sliced off from the cylindrical ingots by making a 2- to 3-mm-deep cut along the circumference on a silicon carbide cut-off wheel followed by hammering. Heating of the specimens during cutting was minimized through water-cooling. Optical metallography was carried out on a Reichert Metavert-368 (Vienna, Austria) microscope. The specimens were etched with freshly prepared 2% nital solution. Scanning electron microscopy (SEM) was carried out with a model JSM 840A scanning electron microscope (JEOL, Tokyo, Japan) at an accelerating voltage of 20 kV. The samples were deep etched in 6% HNO_3 in CCl_4 for this purpose. Electron probe microanalysis (EPMA) was done to study the partitioning behavior of the alloying elements into matrix and carbide. This was done on a Superprobe 733 instrument (JEOL) at an accelerating voltage of 15 kV.

Differential thermal analysis (DTA) was done on a model STA 781 differential scanning calorimeter (Stanton and Redcroft, NJ, USA) using alumina as a reference material. This was carried out primarily to assess the transformation temperature(s) at which the phase transformation(s) occurred while heat-treating was performed. For DTA, powder samples weighing approximately 15 mg and made by turning the as-cast ingot were heated at a rate of 10 °C/min up to 1100 °C.

3. Results and Discussion

Figure 1 is a typical SEM micrograph showing network carbide along austenite grain boundaries obtained after 4 h soaking at 1050 °C followed by air-cooling. EPMA (Table 2) of these carbides revealed that they were chromium-rich (Fe, $Cr)_7C_3$. The formation of M_7C_3 in low Cr alloy can be explained as follows.

The alloy under study contains relatively high phosphorus (Table 1), which is known to segregate in the intercellular space, raising its concentration to a level required to form phosphide eutectic.[13] A liquid phase rich in P, Cr, and C begins to appear at about 950 °C,[14-16] therefore, if the soaking temperature of the alloy is more than this temperature, partial melting may be observed near phosphorus-rich regions. Shin et al.,[17] while studying the liquid film migration in a sintered Fe-Cr-C base alloy, observed the formation of network carbides during solidification of liquid films formed because of the presence of P, Cr, and C as discussed above. The network carbides have also been observed by Thumuki et al.[18] and Suganuma et al.[19] The alloy also contains copper. Because the

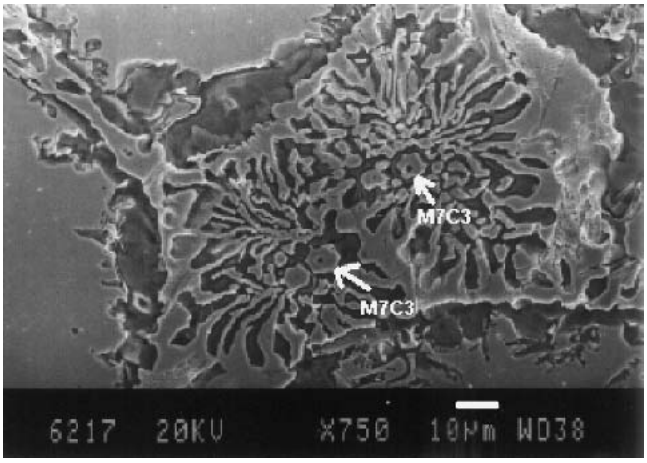

Fig. 1 SEM image showing network carbide M_7C_3 (arrow)

Table 2 Electron Probe Microanalysis of Network Carbide, wt.%

Phase	Fe	C	Si	Cr	Mn	Cu
Network carbides	58.28	12.68	0.04	22.78	9.57	0.04
Austenite matrix	83.03	3.07	2.20	3.14	5.80	1.34

solid solubility of copper is poor except in austenite, it will precipitate out once austenite goes under transformation to other phases. The manganese present may then combine with copper to form a low melting point (873 °C at 34.6% Mn) intermetallic.[20] Copper-rich needles (Fig. 2) observed with SEM-energy-dispersive x-ray analysis (EDAX) analysis in the lower temperature treatments (950 °C, 6 h, air-cooling) confirm this possibility. DTA (Fig. 3) also revealed a peak at 937 °C, indicating possible melting caused by the above-mentioned reasons.

At 1050 °C soaking temperature, two phases exist: austenite and liquid. The liquid is likely to be present at the austenite grain boundaries where the above-mentioned phenomenon would occur. Because chromium has a greater tendency to partition in the carbide rather than in austenite, a large amount of chromium would come out of austenite and would dissolve in the liquid present at the grain boundaries. Concentration of C also increases in the liquid phase, as more and more C is rejected from the austenite because of its lower solubility, compared with carbon present in the alloy. High concentrations of Cr and C will favor the formation of Cr-rich M_7C_3. Figure 4 represents typical hexagonal M_7C_3 carbides. A close examination of these carbides under SEM after deep etching revealed a center-line hole resembling the pencil-like structure described by Pearce.[6]

The following steps can explain formation of such a typical morphology of M_7C_3, as represented in Fig. 5:

1) Nucleation of austenite in the liquid (Fig. 5a);
2) Growth of austenite nuclei (Fig. 5b);
3) Rejection of C and Cr from newly formed austenite due to lesser solubility of these elements in austenite (Fig. 5b);

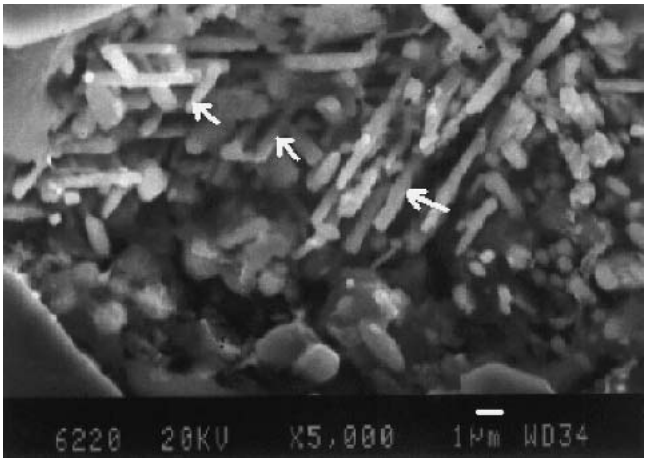

Fig. 2 SEM image showing Cu-rich intermetallic (arrow)

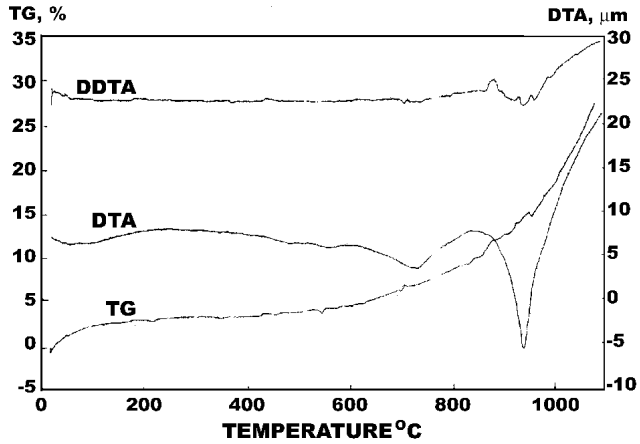

Fig. 3 DTA of the alloy. TG, thermogravimetric; DTA, differential thermal analysis; DDTA, derivative of differential thermal analysis

4) Buildup of C and Cr around austenite (Fig. 5b);
5) Nucleation of M_7C_3 at austenite because of favorable conditions provided by step (4) (Fig. 5c);
6) Movement of C and Cr from the surrounding region in the liquid to M_7C_3 nuclei (Fig. 5c);
7) Growth of M_7C_3 because of step (6) (Fig. 5d);
8) Formation of austenite in the surrounding region of M_7C_3 due to depletion of Cr and C in the adjoining regions (Fig. 5e);
9) Steps (3) to (7);
10) Formation of secondary carbides may take place at M_7C_3 and/or within austenite because of a decrease in the solubility of C and Cr in austenite with a decrease in the temperature (Fig. 5f);
11) Growth of these secondary carbides may join two adjacent M_7C_3, giving a look of a single carbide (Fig. 5f);
12) Transformation of austenite to martensite may take place because of an increase in Ms temperature (Fig. 5f).

The above explanation is also supported by the fact that some M_7C_3 (arrow, Fig. 1) present in the center of rosette-clusters

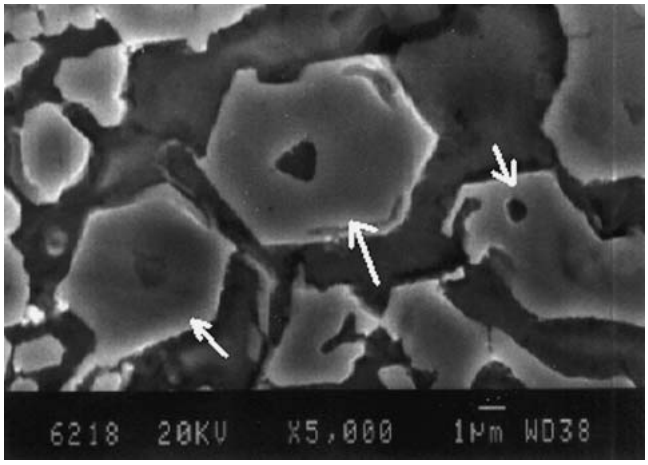

Fig. 4 SEM image showing typical pencil morphology of M_7C_3 carbide (arrow). Dark continuous phase is austenite

have grown to a larger size compared with the nearby M_7C_3, revealing that the nucleation of the M_7C_3 took place initially, followed by formation of other M_7C_3 according to the steps described (Fig. 1). Incomplete growth of M_7C_3 (arrow, Fig. 4), although a core is present, also suggests that nucleation and growth of M_7C_3 takes place after the austenite has grown sufficiently enough to reject the required amount of C and Cr for the formation of M_7C_3 (Fig. 5c).

Formation of rosette-clusters of M_7C_3 (Fig. 1) during solidification of liquid metal can also be explained by the steps described. First, formation of M_7C_3 takes place at a few nucleation sites, followed by their growth as in step (7). Because the second round of nucleation and formation of M_7C_3 take place at a large number of sites according to steps (8) and (9), the sizes of M_7C_3 in the second round are smaller compared with the initially formed M_7C_3. This is followed by another round of formation of M_7C_3. The sizes of these M_7C_3 are still smaller than those in the previous round of M_7C_3. The size of M_7C_3 will depend upon the extent of growth in the available space. Because the available space in the initial round is large, the sizes of M_7C_3 are larger compared with the later rounds of M_7C_3. This process of M_7C_3 formation continues until it encounters another growing cluster of M_7C_3. In the process it forms a rosette structure where each M_7C_3 has an austenite/martensite core resembling a pencil-like structure and is encapsulated by austenite/martensite (Fig. 1).

4. Conclusions

- Segregation of phosphorus in the intercellular regions and formation of copper-rich intermetallic are responsible for the partial melting at austenite grain boundaries.
- M_7C_3 carbide can form because of attainment of a favorable condition in the liquid phase present at the austenite grain boundaries.
- Austenite is the first phase to nucleate and grow in liquid followed by nucleation and growth of M_7C_3 at the newly formed austenite. This reaction proceeds in a manner similar to a eutectic transformation $L \rightarrow M_7C_3 + \gamma Fe$.

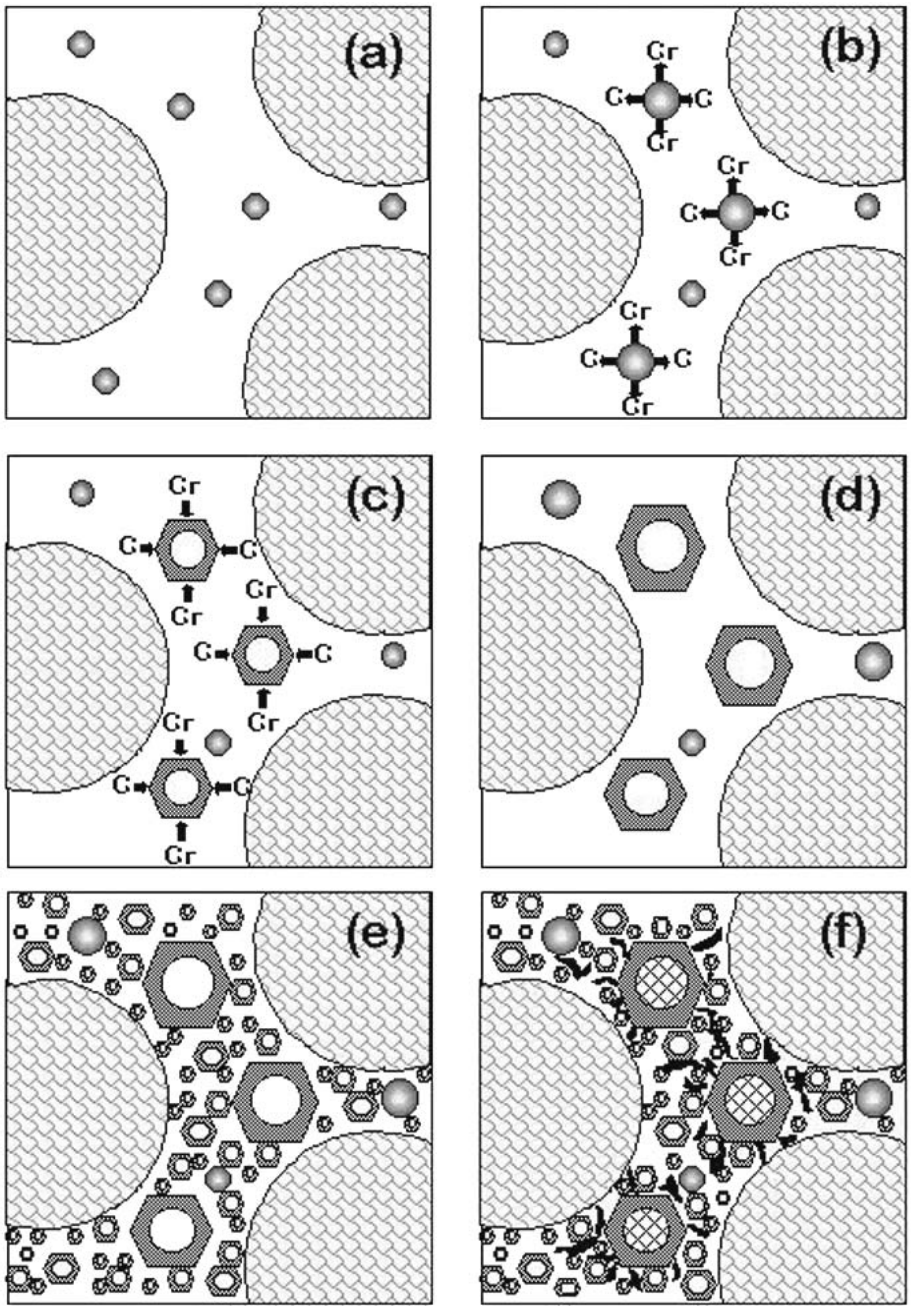

Fig. 5 Schematic representation of formation of pencil morphology of M_7C_3. **(a)** Nucleation of austenite in the liquid; **(b)** growth of austenite and simultaneous rejection of Cr and C; **(c)** nucleation of M_7C_3 at newly formed austenite; **(d)** growth of M_7C_3 caused by movement of Cr and C from adjoining areas; **(e)** fresh nucleation of austenite and its growth followed by nucleation of M_7C_3 and its growth leading rosette-clusters formation; and **(f)** transformation of austenite to martensite due to depletion in Cr and C

- M_7C_3 is enclosed by austenite except where secondary carbide precipitation has joined the two M_7C_3 carbides.

References

1. R.B. Gundlach and D.V. Doane: "Alloy Cast Irons" in *Metals Handbook,* Vol. 1, ASM International, Materials Park, OH, 1990, pp. 85-104.
2. G. Laird II, J.C. Rawers, and A. Adams: "Fractal Analysis of Carbide Morphology in High-Chromium White Cast Irons," *Metall. Trans. A*, 1992, *23A*, pp. 2941-45.
3. M. Doi and T. Miyazaki: "γ Precipitate Morphology Formed Under the Influence of Elastic Interaction Energies in Nickel-Base Alloys," *Mater. Sci. Eng.*, 1986, *78*, pp. 87-94.
4. H. Zhao and G.C. Weatherly: "The Formation of Multi-Domain Precipitates in a Ni-W Alloy," *Acta Metall. Mater.*, 1990, *38*, pp. 2253-60.
5. H. Zhao, K.T. Aust, and G.C. Weatherly: "Morphological Develop-

ment During Ageing of Ni-W Alloys," *Acta Metall. Mater.*, 1992, *40*, pp. 1961-68.
6. N.S. Mishra and S. Ranganathan: "Electron Microscopy and Diffraction of Ordering in Ni-W Alloys," *Acta Metall. Mater.*, 1995, *43*, pp. 2287-302.
7. J.D. Hunt and K.A. Jackson: "Binary Eutectic Solidification," *Trans. Met. Soc. AIME*, 1966, *236*, pp. 843-52.
8. G.A. Chadwick: "The Solidification of Metals, The Iron and Steel Institute" in *Metallography of Phase Transformations,* Butterworths, London, UK, 1967, p. 138.
9. F. Martray: "Choice of Appropriate Compositions for Chromium-Molybdenum White Irons," *AFS Trans.*, 1971, *79*, pp. 121-24.
10. J.T.H. Pearce: "Structure and Wear Performance of Abrasion Resistant Chromium White Cast Irons," *AFS Trans.*, 1984, *126*, pp. 599-622.
11. T. Ohide and G. Ohira: "Solidification of High Chromium Alloyed Cast Irons," *Br. Foundryman*, 1983, *76*, pp. 7-14.
12. W. Steven and A.G. Haynes: *JISI*, 1956, *183*, pp. 349-59.
13. P.C. Liu and C.R. Loper Jr.: "Segregation of Certain Elements in Cast Irons," *AFS Trans.*, 1984, *109*, pp. 289-95.
14. V. Raghavan: "Phase Diagrams of Ternary Iron Alloys" in ASM Handbook, Part 2, ASM International, Metals Park, OH, 1987.
15. N.R. Griffing, W.D. Forgeng, and G.W. Healy: *Trans. AIME*, 1962, *224*, pp. 148-59.
16. R. Benz, J.F. Elliott, and J. Chipman: *Metall. Trans.*, 1974, *5*, pp. 2235-40.
17. H.S. Shin, J.S. Kim, and D.Y. Yoon: "The Liquid Film Migration in a Sintered Fe-Cr-C Base Alloy," *Metall. Trans.*, 1995, *26A*, pp. 1389-93.
18. C. Thumuki, K. Ueda, H. Nakamura, K. Kondo, and T. Suganuma: *Met. Powder Rep.*, 1983, *38*, pp. 433-35.
19. T. Suganuma, H. Nakamura, and T. Hikosaka: *Toyota Technol.*, 1983, *33*, pp. 151-59.
20. Anon: "Alloy Phase Diagrams" in *ASM Handbook,* Vol. 3, ASM International, Metals Park, OH, 1992, p. 2.172.